Research Article

CFD Simulation of a New Dynamic-Static Stirred Model and Its Application in the Leaching Process of Chromite

Bin He,[1] **Lanfeng Guo,**[1] **Renlong Liu,**[1] **Facheng Qiu** [ORCID],[2] **and Xuejun Quan**[2]

[1]*School of Chemistry and Chemical Engineering, Chongqing University, Chongqing 400044, China*
[2]*School of Chemistry and Chemical Engineering, Chongqing University of Technology, Chongqing 400054, China*

Correspondence should be addressed to Facheng Qiu; qiufachengandl@126.com

In the liquid phase oxidation leaching process of chromite salt, a new dynamic-static combined stirred mode is proposed. That is, a static cylindrical baffle is fixedly installed at a certain radius from the stirred blade to control the vicinity of the blade. The CFD numerical simulation method is mainly used to investigate the effect of dynamic-static combined mode on the flow field distribution. Meanwhile, the velocity distribution and trailing vortex near the blade are analyzed. Finally, the differences between traditional stirred blade and dynamic-static combined stirred blade in the oxidation leaching process of chromite are compared. The results show the new dynamic-static combined stirring mode can effectively improve the flow field distribution, reduce the occurrence of "dead zones" in the flow, and increase the chromite leaching efficiency. The leaching time can be reduced from 300 to 240 min, and the chromium-leaching rate has reached up to 99%.

1. Introduction

Chromium and its compounds are of great importance for chemical industry and metallurgy [1]. Production efficiency and clean production have attracted more and more attention in the production process of chromate. In terms of the leaching process of chromite, it is a fine particle size powder and an extreme high alkali concentration is adopted. The solid-liquid mixed system has a slurry state with extremely high viscosity and density [2]. When the leaching process of chromite is further considered, how to improve the mixing state of the reaction system is a crucial problem to be solved. Significantly, the configuration of the agitator, which affected the flow state of the fluid and the solid-liquid mixing efficiency, is the vital part of reactor in the alkali leaching process.

Recently, more and more studies about the optimization of the agitator have been published in either temporal or spatial terms [3]. These enhanced mixing methods mainly include turbulence, time-varying rotation, eccentric rotation, reciprocating stirring, and so on [4]. Actually, the enhanced mixing methods are to disrupt the periodicity of the fluid particle motion trajectory by disturbing the internal dynamics of the fluid. Lamberto et al. [5] utilized the method of unsteadily rotational impeller speed to distribute flow field, and the higher mixing efficiency is obtained with frequent disturbance occurring. Nomura et al. [6] used the method of periodically changing the rotating direction of the impeller to achieve a better mixing efficiency. Moreover, Zhang et al. [7] employed the method of eccentric stirring to enhance the mixing efficiency in highly viscous liquids system. Liu et al. [8] introduced a rigid-flexible combination impeller to improve utilization rate of energy. In this present work, a novel stirring mode, namely, dynamic and static coupling modes, was proposed to enhance the degree of mixing in the unbaffled system. The detailed structure is shown in Figure 1.

The hydrodynamics behavior is of vital importance for the structure design and operation parameters of agitator [9]. Then, the computational fluid dynamics (CFD) has been considered as a powerful tool in analyzing the flow characteristics in a stirred tank [10]. Li and Xu [11] carried out a numerical simulation to investigate the turbulent flow with free-surface vortex in an uncovered unbaffled stirred tank. Li
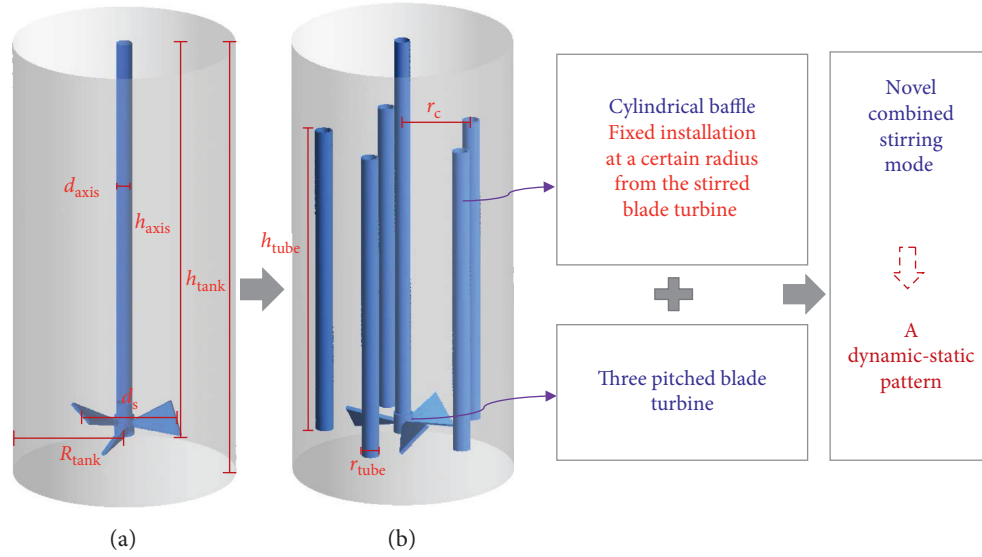
FIGURE 1: Schematic of the stirred tank. (a) Traditional chromite leaching stirred reactor. (b) Dynamic-static combined chromite leaching stirred reactor.

et al. [12] conducted a computational fluid dynamics simulation study on the relationship between the impeller speed, the impeller clearance, and the liquid level in the hollow shaft. It was found that the CFD simulation method was conducive to optimize agitator structure and operation parameters.

In this paper, the dynamic and static combined stirred method was proposed to improve the mixing state in an unbaffled tank system. For the current research section, the liquid-phase mixing system was mainly considered via a CFD simulation method using a k-ε turbulence model. The major aim of the present work was to understand the effect of the novel stirred method on the mixing behavior and deepen the cognition of flow field evolution in the process of liquid phase mixing process. Meanwhile, the velocity distribution and the trailing vortex near the impeller were all analyzed. Finally, the differences between traditional impeller and dynamic-static coupling stirring in the oxidation leaching process of chromite are compared. This research can provide the basic data for the optimization design of chromite leaching reactor.

2. Simulation Section

2.1. Geometric Model and Meshing. The geometric model and computational domain are shown in Figures 1 and 2, respectively. In the process of numerical simulation, a three-pitched blade impeller with the diameter 55.00 mm was used. The maximum cross-sectional width of the blade was 19.00 mm, and the minimum cross-sectional width close to the stirring shaft was 8.00 mm. The off-bottom clearance of impeller was 20.00 mm. The five tubes with the diameter 9.30 mm and height 150.00 mm were, respectively, fixed within a radius of a certain distance from the stirred shaft, which were evenly distributed in a regular pentagon. The ratio of the radius of the five circular pipes to the radius of the stirred tank is 70.00 mm. In order to improve the

accuracy of simulation, mesh refinement processing was performed on the impeller area and the area of the tubes. The grid number of the traditional chromite leaching stirred reactor (Figure 2(a)) was 67457, and the grid number of the dynamic-static combined chromite leaching stirred reactor (Figure 2(a)) was 80970. The structural parameters of the geometric model during the simulation are shown as Table 1.

2.2. Governing Equations. In the numerical simulation process, the fluid flow satisfied the conservation of mass and momentum. Our current work did not involve energy conversion, so energy conservation was not considered. The mathematical expression of conservation were given below [13]:

Mass equations:

$$\frac{\partial \rho}{\partial t} + \frac{\partial}{\partial x_i} (\rho u_i) = 0. \tag{1}$$

Momentum equations:

$$\frac{\partial}{\partial t} (\rho u_i) + \frac{\partial}{\partial x_i} (\rho u_i u_j) = -\frac{\partial p}{\partial x_i} + \frac{\partial \tau_{ij}}{\partial x_j} + \rho g_i + F_i, \tag{2}$$

where P was static pressure, τ_{ij} was stress tensor, g_i and F_i were the gravitational volume force and external volume force in the i direction, respectively. The stress tensor was given as follows:

$$\tau_{ij} = \left[\mu \left(\frac{\partial u_i}{\partial x_j} + \frac{\partial u_j}{\partial x_i} \right) \right] - \frac{2}{3} \mu \frac{\partial u_l}{\partial x_l} \delta_{ij}. \tag{3}$$

The equation describing the turbulent motion adopted time averaging (Reynolds, RANS) and introduced new unknowns, and the equation became unclosed. The method of eddy viscous mode was adopted to close the equation. In addition, the velocity consisted of average velocity $\overline{u_i}$ and fluctuation velocity u_i'.
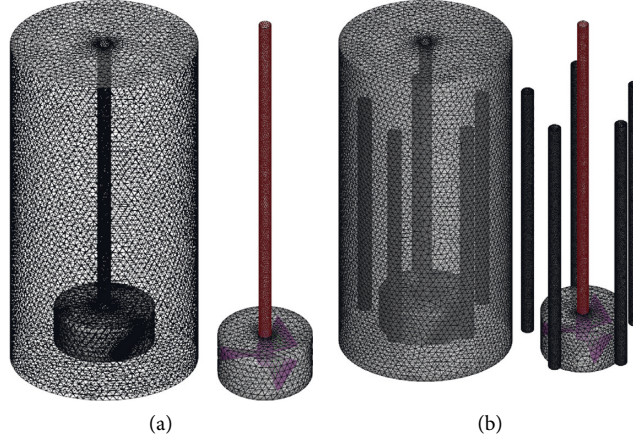
FIGURE 2: Computational domain and mesh grid. (a) Traditional chromite leaching stirred reactor. (b) Dynamic-static combined chromite leaching stirred reactor.

TABLE 1: Geometric dimensions of tank.

Symbol	Value	Unit	Comment
d_{axis}	7.74	mm	Stirred shaft diameter
h_{axis}	210.00	mm	Stirred shaft height
h_{tank}	565.56	mm	Stirred tank height
d_s	55.00	mm	Stirred impeller diameter
R_{tank}	210.00	mm	Stirred tank radius
r_c	70.00	mm	Fixed position radius of circular tube
d_{tube}	9.30	mm	Circular tube diameter
h_{tube}	150.00	mm	Circular tube height

$$u_i = \overline{u_i} + u_i', \tag{4}$$

$$-\rho\overline{u_i'u_j'} = \mu\left(\frac{\partial u_i}{\partial x_j} + \frac{\partial u_j}{\partial x_i}\right) - \frac{2}{3}\left(\rho k + \mu\frac{\partial u_l}{\partial x_l}\right)\delta_{ij}, \tag{5}$$

where μ was turbulent viscosity, δ_{ij} was Kronecker delta symbol, when the $i = j$, $\delta_{ij} = 1$. When the $i \neq j$, $\delta_{ij} = 0$. k was turbulent kinetic energy.

$$k = \frac{\overline{u_i'u_j'}}{2}. \tag{6}$$

Based on the equation of turbulent kinetic energy k, an equation about turbulent dissipation rate ε was introduced to form a k-ε two equation model. Turbulent dissipation rate ε was defined as follows [14]:

$$\varepsilon = \frac{u}{\rho}\overline{\left(\frac{\partial u_i'}{\partial x_k}\right)\left(\frac{\partial u_j'}{\partial x_k}\right)}. \tag{7}$$

Then, the turbulent viscosity μ can be defined as a function of k and ε.

$$\mu = \rho C_\mu \frac{k^2}{\varepsilon}. \tag{8}$$

According to the above analysis, when the fluid was incompressible and phase change was not considered, the standard k-ε equation [15] can be defined as follows:

$$\frac{\partial(\rho k)}{\partial t} + \frac{\partial}{\partial x_i}(\rho u_i k) = \frac{\partial}{\partial x_i}\left[\left(\mu + \frac{\mu_\tau}{\sigma_k}\right)\frac{\partial k}{\partial x_i}\right] + \frac{1}{2}(P_{ii} + G_{ii}) - \rho\varepsilon, \tag{9}$$

$$\frac{\partial(\rho\varepsilon)}{\partial t} + \frac{\partial}{\partial x_i}(\rho u_i\varepsilon) = \frac{\partial}{\partial x_j}\left[\left(\mu + \frac{\mu_\tau}{\sigma_\varepsilon}\right)\frac{\partial\varepsilon}{\partial x_j}\right] + C_{1\varepsilon}\frac{1}{2}(P_{ii} + C_{3\varepsilon}G_{ii}) - C_{2\varepsilon}\rho\frac{\varepsilon^2}{k}, \tag{10}$$

where $C_{1\varepsilon}$, $C_{2\varepsilon}$, C_μ, σ_k, and σ_ε were constants. Their values were equal to 1.44, 1.92, 0.09, 0.82, and 1.0, respectively.

2.3. Simulation Method and Boundary Conditions. In order to deeply explore the flow behavior in the reactor under the new dynamic-static stirring mode, the standard k-ε two equation model in the eddy viscosity model was used to simulate and describe its change. The description of the mathematical model was shown in equations (1)–(10). In the

simulation process, the multiple frames of reference (MRF) method was adopted, and the region where the blades are located was set as the rotating region, and the other parts of the fluid were set as the static region. The division of rotating and static region is shown in Figure 3. This work mainly employed ANSYS FLUENT 15.0 by using steady-state solution calculation, the simulation system was single-phase, which can provide a help for reactor structure optimization under a clean water experiment. Thus, the medium was set as liquid water. The pressure-velocity coupling solution
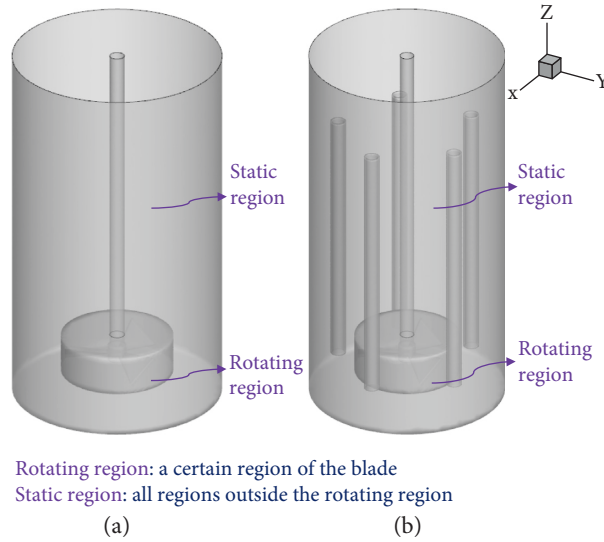
FIGURE 3: The division of rotating and static region. (a) Traditional chromite leaching stirred reactor. (b) Dynamic-static combined chromite leaching stirred reactor.
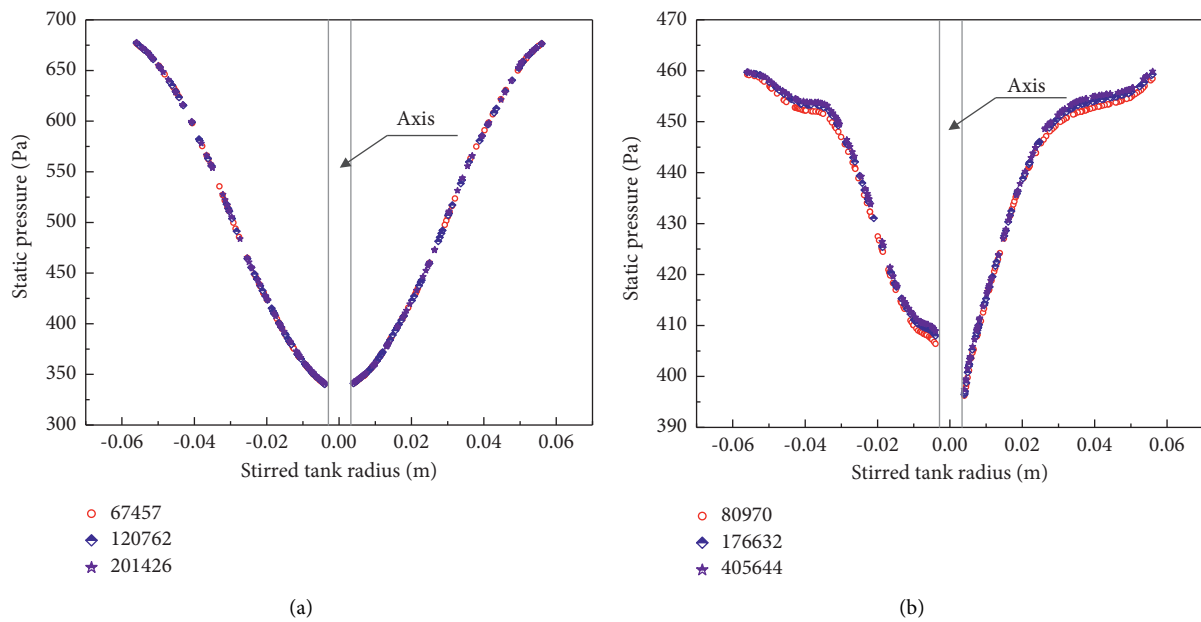

FIGURE 4: The effect of mesh number on the static pressure. (a) Traditional chromite leaching stirred reactor. (b) Dynamic-static combined chromite leaching stirred reactor.

method was SIMPLE. Impeller velocity was set to 900 rpm, and the stirred direction was counterclockwise. The discretization scheme of the convective term is the second-order upwind and the convergence residual was set to 10^{-5}. Both the wall of the stirred tank and the circular tube fixed in the reactor (equivalent to the role of the static blade in the fluid flow process) were set as static walls. Meanwhile, the transfer of mass and energy was realized by the internal interface.

3. Results and Discussion

3.1. Mesh Independence and Model Verification. The origin of the coordinate calculated by the numerical simulation was set at the lowest end of the center line of the stirring shaft, and downward was positive. There were many sharp areas in the geometric model, and then the unstructured hybrid mesh type was used when dividing the mesh. When investigating the influence of different mesh numbers on the
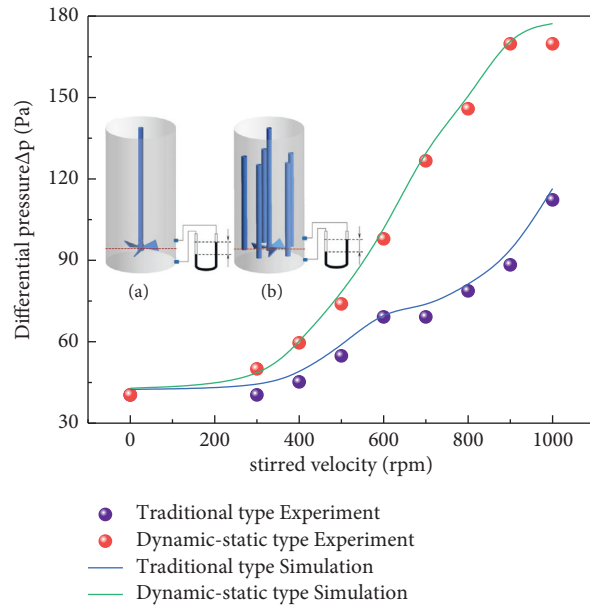
FIGURE 5: Change of pressure difference under experimental measurement and numerical simulation.
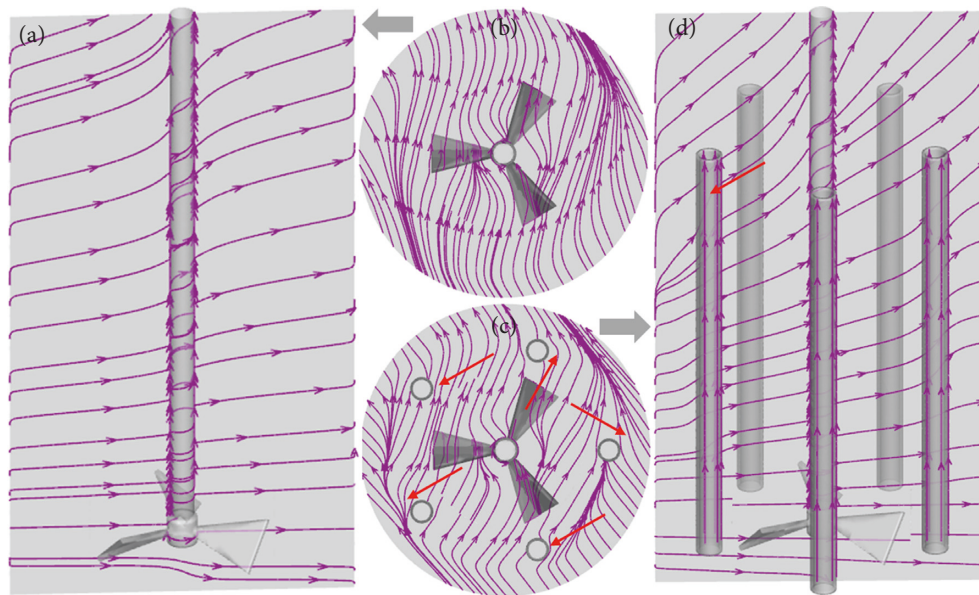

FIGURE 6: The distribution of fluid flow traces in the tank. (a, b) Flow trajectory on the vertical and horizontal planes under traditional stirred tank. (c, d) Flow trajectory on the vertical and horizontal planes under dynamic-static combined stirred tank.

calculation process, the mesh division of the traditional stirred reactor was 67457, 120762, 201426, and the grid division of the dynamic-static coupled stirred reactor was 80970, 176632, and 405644. The influence of mesh number on the static pressure distribution in the vertical direction was carried out. As shown in Figure 4, the effect of the number of mesh on the static pressure distribution in the simulation system was almost negligible. After calculation, the error under different grids was within ±5%. Therefore, in order to save the calculation cost, the meshes of the traditional stirred reactor and the dynamic-static coupled stirred reactor were selected as 67457 and 80970.

From the standpoint of model verification, a plexiglass kettle of the same scale as the liquid phase oxidation reaction was used to verify the model. The pressure difference of the two stirring systems at different impeller velocity was measured by a U-type differential pressure gauge external to the tank wall. Taking the cross section where the stirring blade was located as the center, two symmetrical positions on the wall with a height difference of 0.05 m in the vertical direction were the measuring points. In particular, the average value after the three measurements were used in measurement process. As shown in Figure 5, the pressure difference between the two stirring modes under the
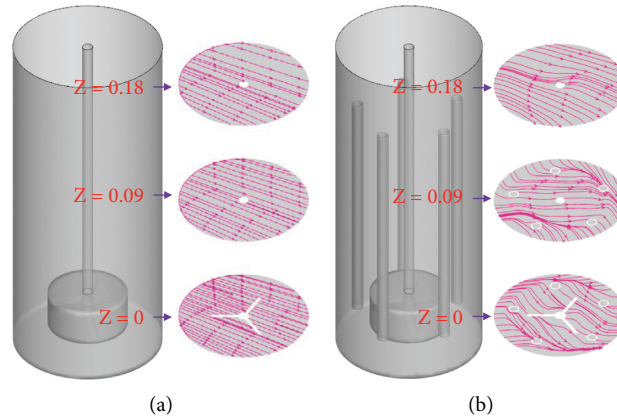
FIGURE 7: The distribution of fluid flow traces on different horizontal planes in the tank. (a) Traditional stirred tank. (b) Dynamicstatic combined stirred tank.
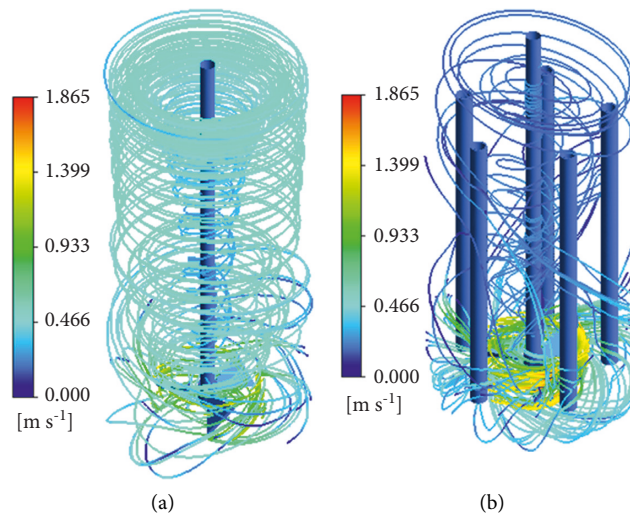

FIGURE 8: Three-dimensional trajectory distribution of fluid flow in the tank (displayed by the velocity). (a) Traditional stirred tank. (b) Dynamic-static combined stirred tank.

simulated conditions was basically consistent with the experimental measurement, and the maximum error was also within 10.78%. It can also be seen from Figure 5 that the pressure difference under dynamic-static coupled stirring is greater than that of the traditional stirring mode.

3.2. Flow Filed. Figure 6 indicated the distribution of fluid flow traces on the vertical and horizontal planes in the tank. As shown in Figures 6(a), 6(d), the flow trajectory of the fluid on the vertical plane conformed to the flow pattern of the axial flow blade, that is, a large global axial circulation was generated. The axial flow of the dynamic-static combined blade on the vertical plane was more obvious, that is, the obvious upward flow in Figure 6(d). In terms of the flow trajectory of the fluid near the circular tube, the fluid moved upward along the tube, and then the flow could be optimized. As shown in Figures 6(b), 6(c), from the standpoint of the flow trajectory of the horizontal plane in the tank, the flow trajectory of the fluid in the traditional stirred tank was relatively symmetric, that is, there was an obvious coherent

flow. For the dynamic-static stirred tank, the fluid flow trajectory had a large disorderly flow, especially the fluid near the tube.

In order to further investigate the influence of the circular tube on the fluid flow in the stirred tank, the distribution of the fluid flow trajectory at different horizontal positions was studied. Figure 7 shows the fluid flow patterns at three horizontal plane positions, that is, $Z = 0$ (the plane where the blade was located), $Z = 0.09$ (the middle position area of the circular tube), and $Z = 0.18$ (the area without the circular tube). As shown in Figure 7, the fluid flow trajectory under the traditional blade showed a relatively obvious orderly and symmetrical distribution, while the orderly flow of the fluid flow trajectory under the combined dynamic and static stirring mode was broken. The fluid near the circular tube had an obvious movement around the tube, and then this circumfluence also extended to the area outside the circular tube ($Z = 0.18$).

Figure 8 shows the three-dimensional trajectory distribution of fluid flow in the tank. As shown in Figure 8(a), the fluid flow in the traditional three-pitched-blade stirred reactor
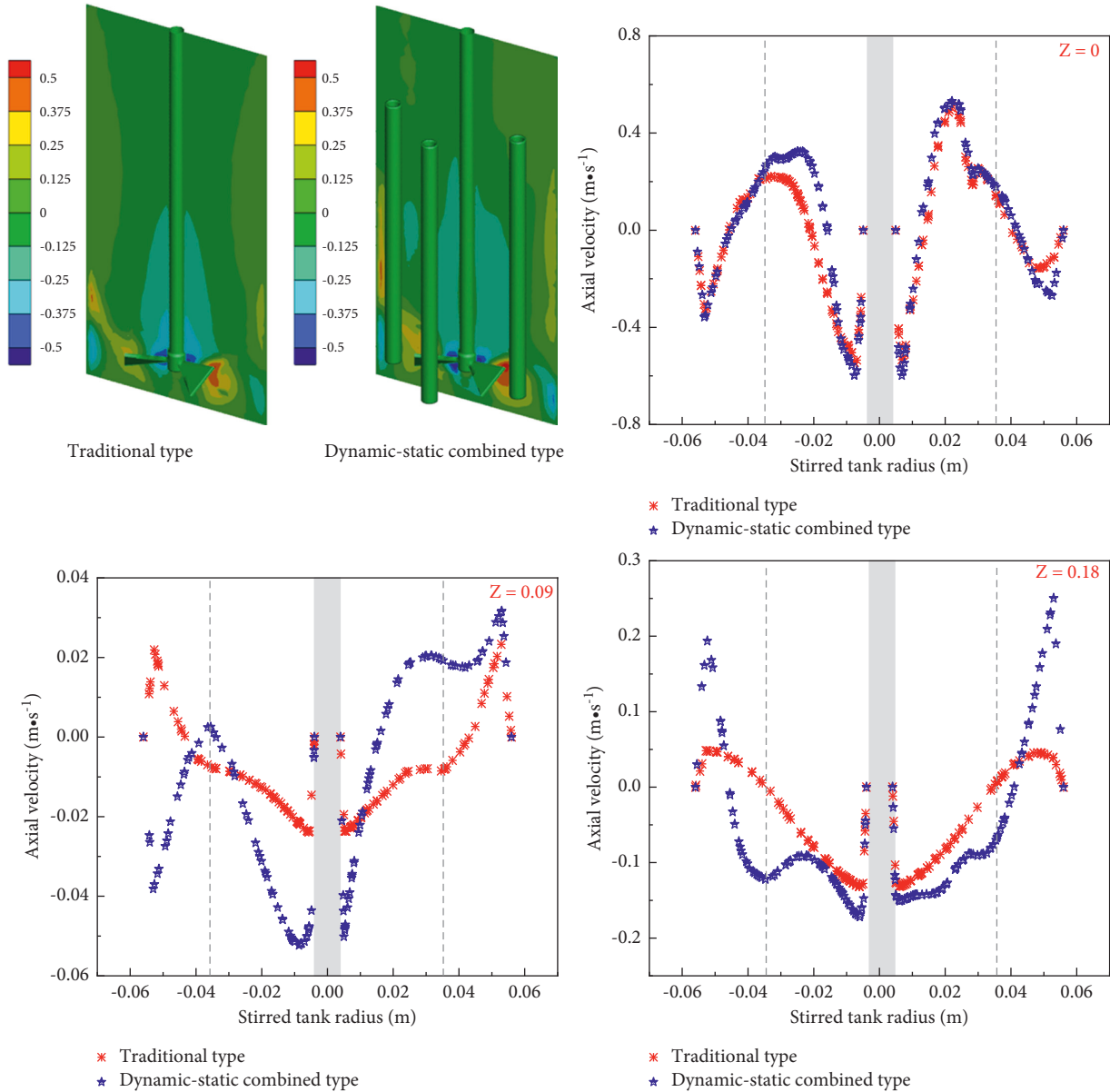
FIGURE 9: The axial velocity distribution at different planes ($Z = 0$, $Z = 0.09$, $Z = 0.18$).

performed a large shear motion in the whole tank, and the fluid flow behavior was dominated by orderly symmetry. As shown in Figure 8(b), when the circular tube was introduced, the fluid starting from the blade will encounter obstacles when flowing through the tube, causing the fluid to flow around the tube. At a certain velocity, this flow method can increase fluid particles collision, destroy the symmetrical flow field in the tank and reduce the appearance of stirring "dead zone."

In a word, when the fluid flowed through the tube, the fluid moved around the tube obviously, and the randomness of the fluid flow was increased under the coupling action of the axial flow impeller. Under the stirring action of the axial flow paddle, the tube in the static state can form a function similar to a "circular tube," which could increase the axial flow in the tank, improve the disordered flow of the fluid, and break the symmetrical flow field distribution in the tank.

3.3. Velocity Distribution. Figures 9–11 show the axial, radial, and tangential velocity distribution in the tank under different stirred models, respectively. In particular, in order to consider the effect of the circular tube on the flow field, the position of the circular tube was marked with a gray dashed line in the following figures.

As shown in Figure 9, the absolute value of the axial velocity in the dynamic-static combined stirred model was larger than that of the traditional three-pitch blade. From the characteristics of axial velocity fluctuations at different planes, there was a significant change in the axial velocity distribution near the tube. When compared with traditional stirred tank at $Z = 0$ and $Z = 0.09$, the axial velocity of the dynamic-static combined stirred model near the tube had a different wave peak distribution. When $Z = 0.18$, the axial velocity near the tube had the characteristics of wave trough
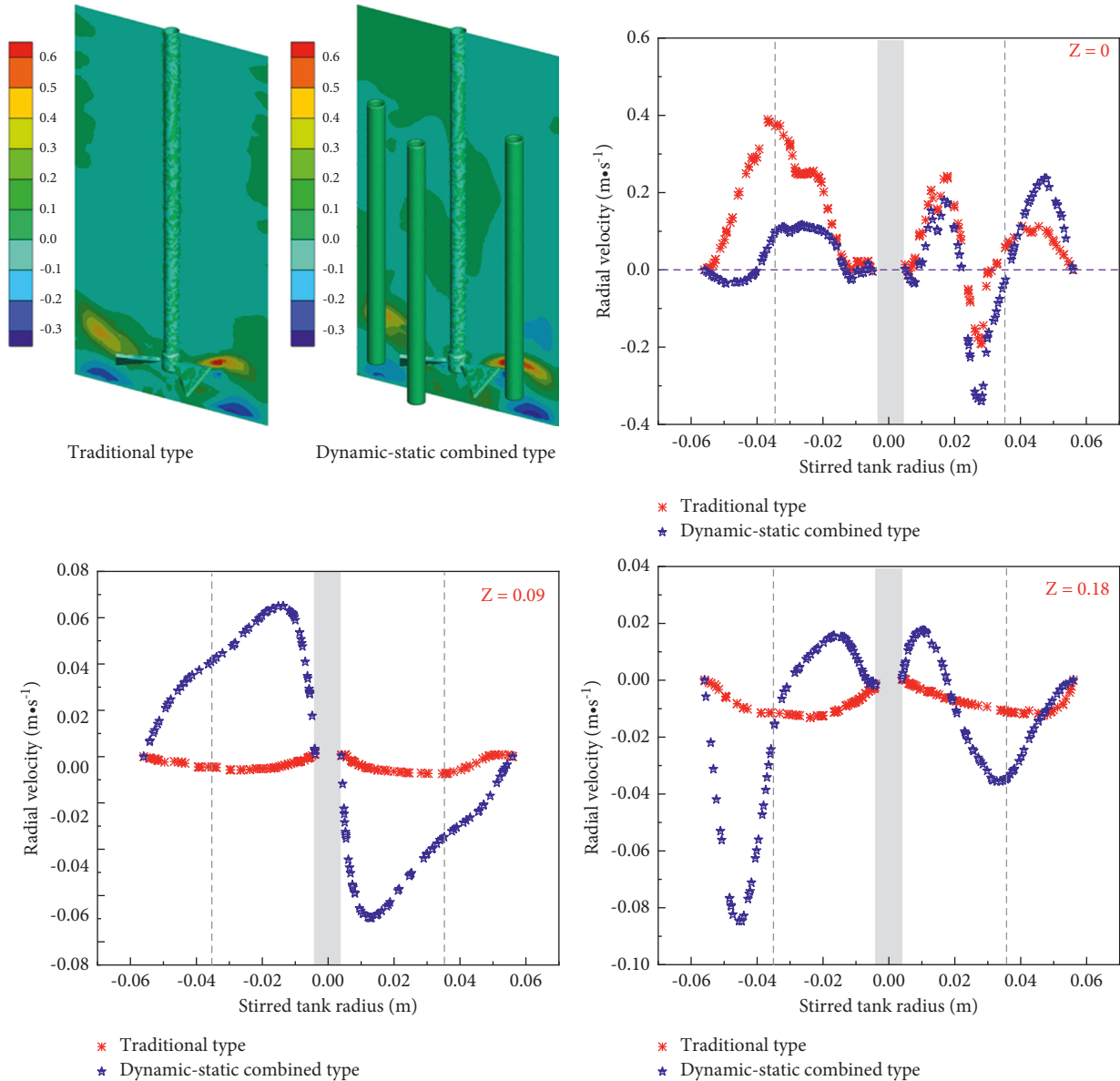
FIGURE 10: The radial velocity distribution at different planes ($Z = 0$, $Z = 0.09$, $Z = 0.18$).

distribution. That meant the tube could affect the flow of fluid beyond it.

Figure 10 indicates the radial velocity distribution at different planes ($Z = 0$, $Z = 0.09$, $Z = 0.18$) in the stirred tank. When it was at the $Z = 0$ plane, that is, when the stirred blade was located, the stirred blade had an obvious effect on the fluid and the flow was relatively turbulent. This situation would result in the multiple radial velocity distributions with zero velocity in both types of blade modes. When it was at the plane $Z = 0.09$, the radial velocity in the dynamic-static mode had large fluctuations. That is, there was a peak distribution in the area between the stirred shaft and the circular tube. There was no significant change in the radial velocity under the traditional three-pitch blade condition.

When it was at the plane $Z = 0.18$, two peaks appeared in the area between the stirred shaft and the tube. Meanwhile, two wave trough distributions appeared between the tube and the inner wall of the stirred tank.

Figure 11 expresses the tangential velocity distribution at different horizontal planes in the tank. As shown in Figure 11, the tangential velocities were all negative values, which were opposite to the counterclockwise direction set by the boundary conditions. There was an obvious phenomenon that the tangential velocity in the dynamic-static coupled stirred reactor was lower than that in the traditional stirred reactor. Generally, in an unbaffled tank, the greater tangential velocity could result in forming a "swirling" flow easily. Therefore, the dynamic-static stirred mode can
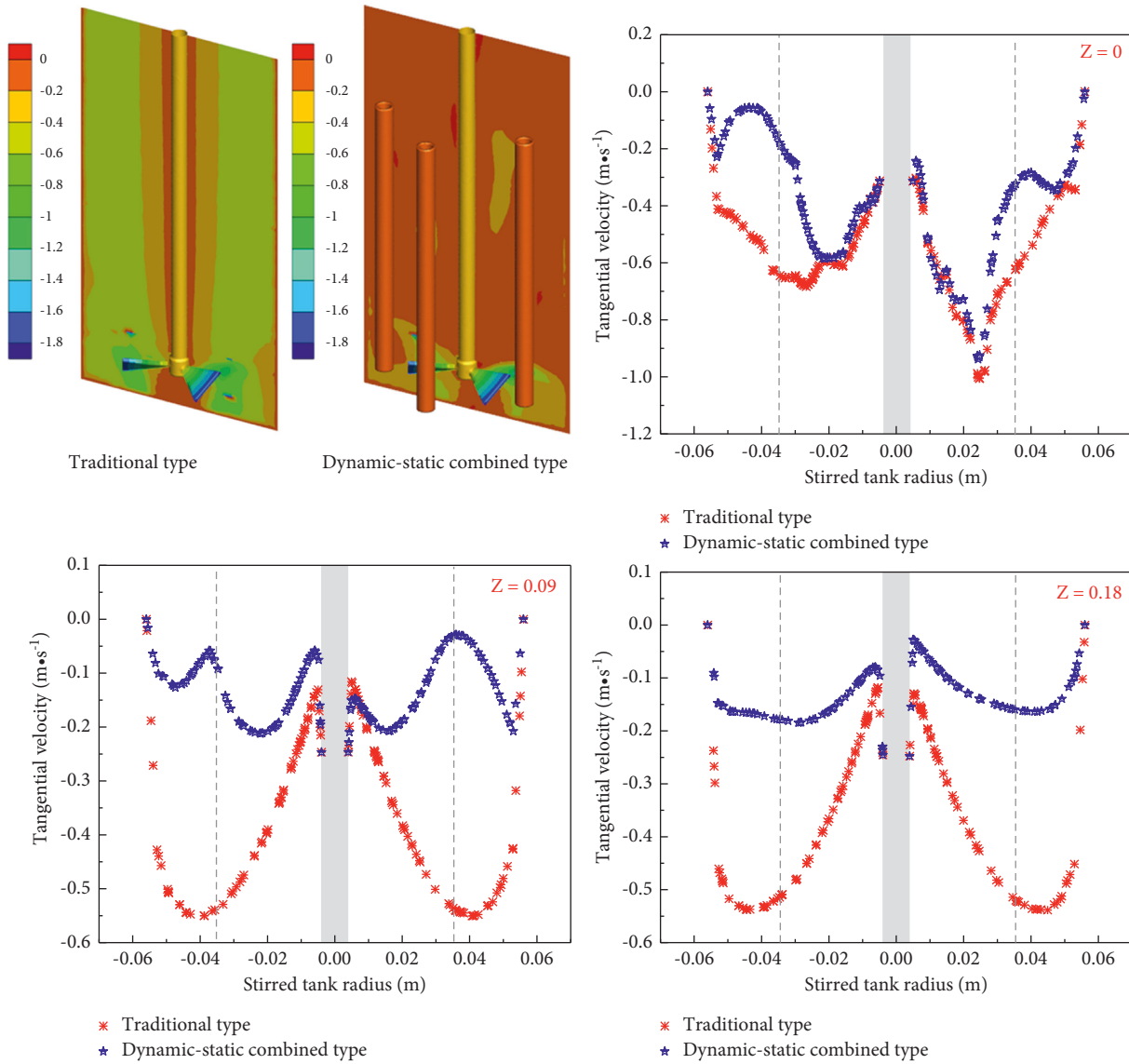
Figure 11: The tangential velocity distribution at different planes ($Z = 0$, $Z = 0.09$, $Z = 0.18$).

effectively reduce the tangential velocity, decrease the probability of the fluid "swirling" flow, and destroy the "dead zone" in the flow process.

3.4. Velocity Iso-surface Distribution.

In order to further investigate the characteristics of the three-dimensional velocity distribution in the tank, the different velocity iso-surfaces (iso-surface value was equal to 0.3, 0.5, 0.7, 0.9 m/s, respectively) were taken into consideration. As shown in Figure 12, when the velocity iso-surface was equal to 0.3 m/s, a relatively obvious "swirling" flow state was formed in the traditional stirred tank. The "swirling" flow in the new dynamic-static stirred tank was broken by the installed circular tube. When the velocity iso-surface was equal to 0.5 m/s, the "swirling" flow area formed in the traditional stirred tank gradually moved to the direction of the stirred axis. When the velocity iso-surface was equal to 0.7 m/s and

0.9 m/s, the distribution area of the velocity iso-surface in the two stirred modes was mainly concentrated near the blade.

3.5. Trailing Vortex Distribution.

Figure 13 indicates the cloud diagram of the trailing vorticity distribution near the blades. It can be seen from Figure 13 that as the vorticity value increased, the trailing vortex at the tip of the blade gradually decreased. When the vorticity value was equal to 0.03, compared with the traditional stirred tank, the trailing vortex in the area behind the stirred blade under the dynamic-static stirred tank was reduced, and the trailing vortex structure was changed. When the vorticity value was equal to 0.04, the trailing vortex near the stirred shaft under the dynamic-static combined stirred tank was significantly reduced or even disappeared. When the vorticity value was equal to 0.05, the trailing vortices in both stirred tanks were
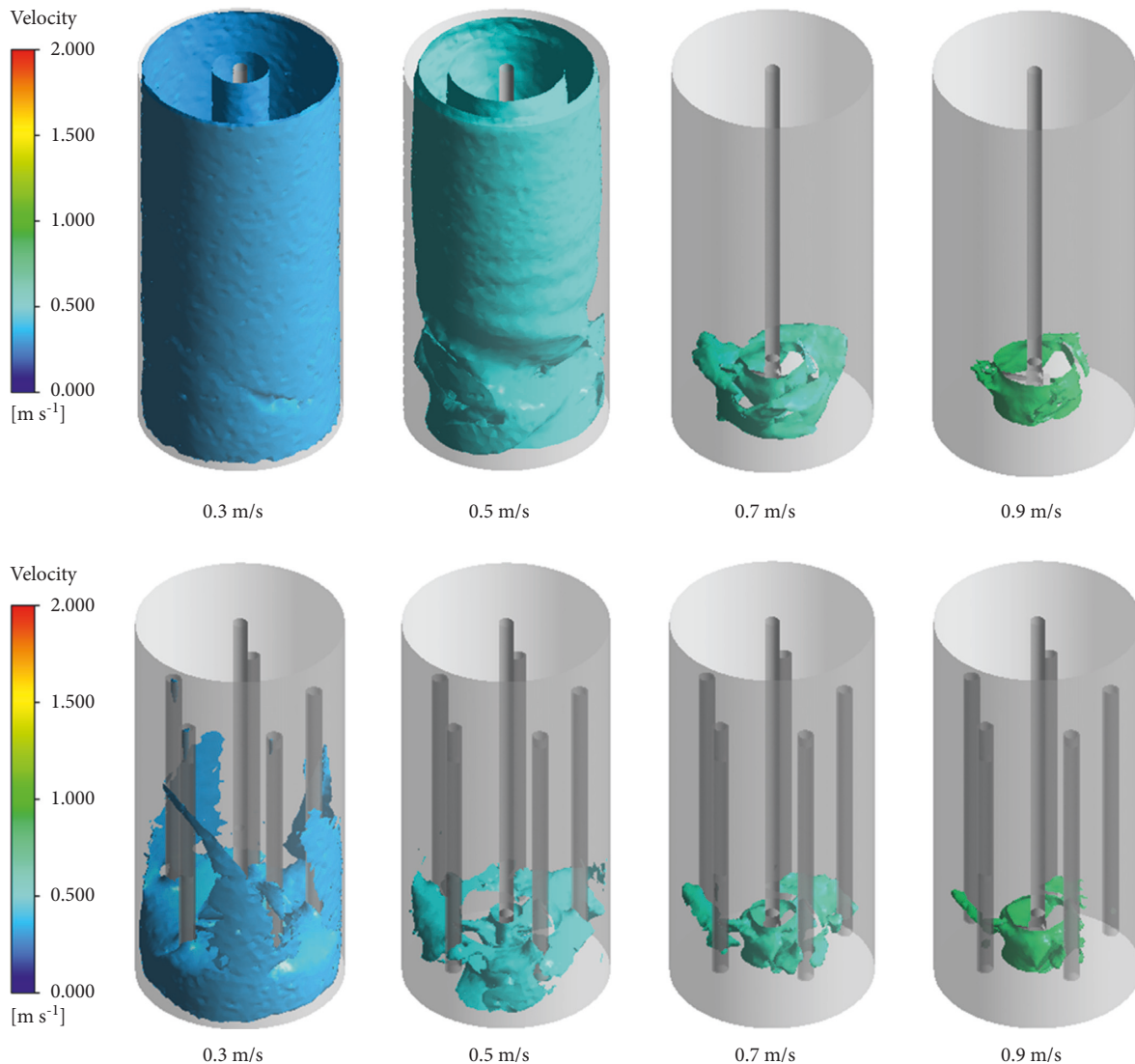
FIGURE 12: Cloud diagrams of the velocity iso-surface distribution in the tank.

further reduced. In a word, the dynamic-static combined stirred model could reduce the trailing vortex near the stirred blade and the stirred shaft.

3.6. Analysis of Solid-Liquid Mixing Behavior. In addition, in order to obtain a better understanding of chromium leaching process, the simulation of solid-liquid two-phase flow was carried out. In this work, the Eulerian–Eulerian multiphase model was employed to simulate the mixing behavior of solid-liquid two phases [16]. In the simulation process, the initial volume distribution of solid particles is defined as 60%. The actual physical parameters of chromite are defined as solid particles. The diameter of chromite particles was 45 μm. In this section, Figure 14 indicates the overall solid holdup distribution in the tank and the solid holdup distribution near the impeller. It can be seen from the figure that the solid particles mainly rotate with the main fluid under the traditional stirring system.

Meanwhile, there was an obvious vortex phenomenon. On the contrary, in the dynamic-static coupling stirring mode, the solid particles have a better overall distribution, and the spinning phenomenon is obviously restrained. This result was basically consistent with the above velocity and vorticity analysis.

3.7. Analysis on the Effect of Chromite Leaching Process. In the whole chromite leaching process, the microleaching kinetic mathematical model revealed the chromite concentration of the group was one of the key influencing factors. The concentration of chromite in the reactor was closely related to the whole solid-liquid mixing effect. Thus, in order to enhance the mixing efficiency of solid-liquid system, a dynamic-static coupling model was proposed to strengthen the whole mixing process. The detailed microleaching kinetic mathematical model can be expressed as follows [17]:
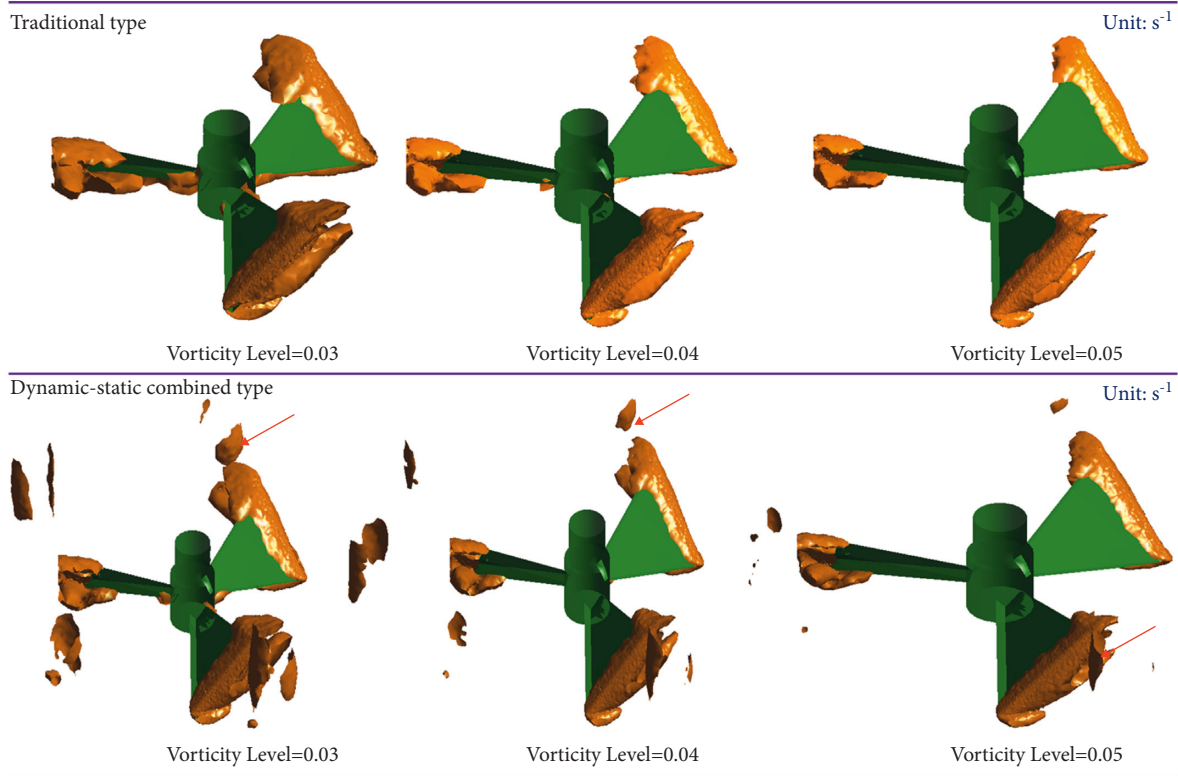
FIGURE 13: Cloud map of the trailing vortex distribution near the blades in the tank.

$$1 - \frac{2}{3}X - (1 - X)^{2/3} = \frac{D_S C_{A0}}{2\rho r_0^2}t, \tag{11}$$

where X denotes the Cr leaching efficiency, r_0 denotes the radius of the chromite ore particle, D_s denotes the mass transfer coefficient of the group, t denotes the reaction time, C_{A0} denotes the concentration of the group at $t = 0$, and ρ denotes the density of the chromite ore particle.

As mentioned above, the new dynamic-static combination stirred tank can reduce the occurrence of "swirling" flow and help improve the energy transfer efficiency in the tank. In order to further confirm the effect of the new stirred tank, it was applied to the chromite leaching process, and the difference in the effect of the two stirred tanks in the chromite leaching process was compared. The stirred velocity was set as 900 rpm. The other experimental conditions and the determination method of Cr(VI) content were as in literature [18].

The chromium-leaching rate under the two stirring modes varied with the reaction time as shown in Figure 15. After the reaction in the reactor device using only traditional stirred blades, the maximum chromium-leaching rate in the leaching solution was only 90%. The total leaching process took 300 minutes. After using the dynamic-static stirred blade, the chromium-leaching rate had reached 99% in 240 min. In a short period of 60–120 min, the leaching rate in the dynamic-static combined stirred reactor was about two times higher than that in the traditional stirred reactor. As mentioned in the previous simulation, under the traditional stirred blade, the fluid in the reactor is prone to swirling flow. That is, a swirling flow state centered on the stirred shaft would be formed during stable operation process. This swirling phenomenon was not conducive to the mixing of the components in the fluid. In the process of solid-liquid mixing, the new stirring mode can effectively improve the solid-liquid dispersion behavior in the system and break the "swirling" phenomenon mentioned above, so as to achieve the purpose of enhanced leaching. The enhanced solid-liquid mixing analysis is shown in Figure 16. Thus, the dynamic-static combined stirred reactor could effectively break the symmetrical flow field, cause fluid interface instability, and then enhance the chromium leaching rate.
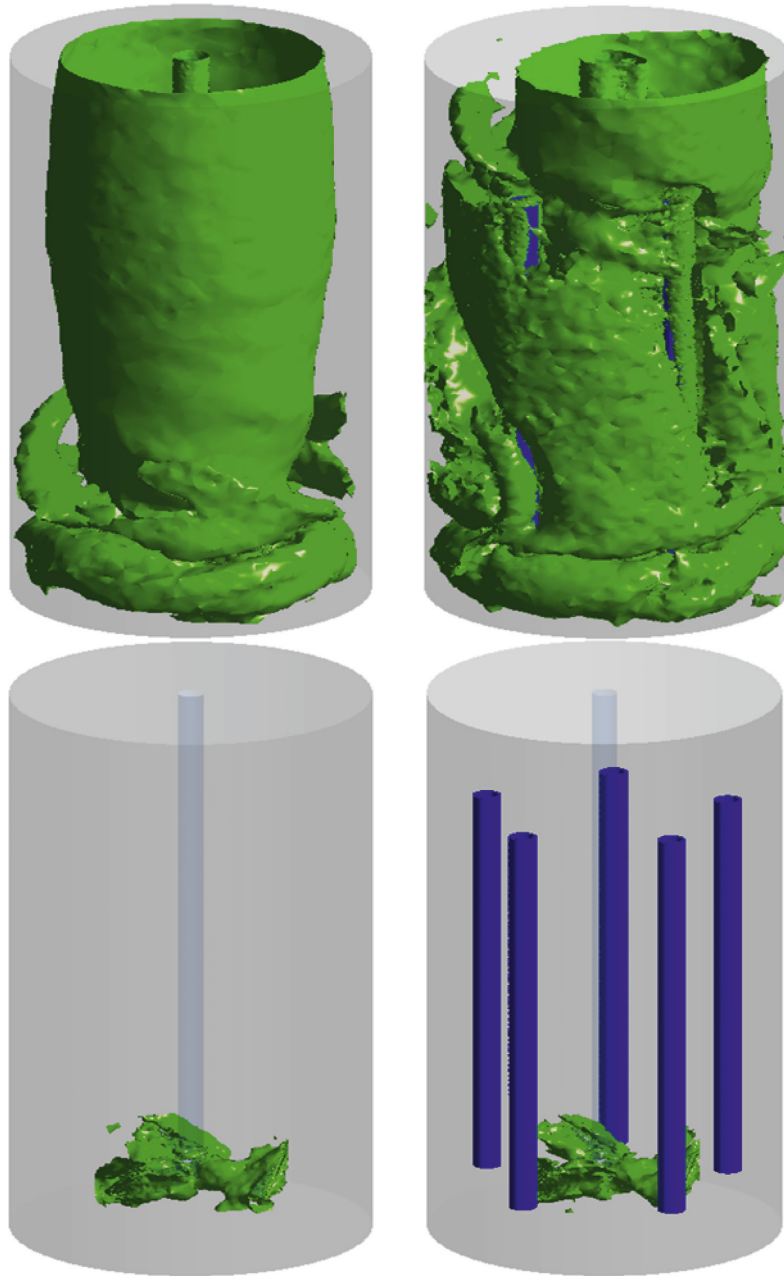
FIGURE 14: The overall solid holdup distribution in the tank and the solid holdup distribution near the impeller.
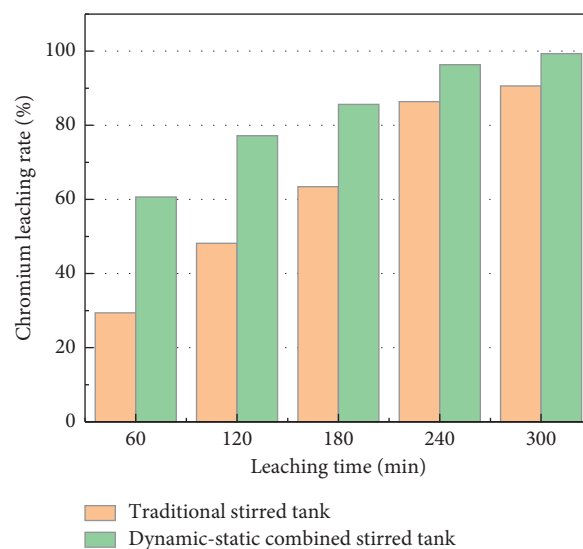
Figure 15: The chromium-leaching rate under the two stirred tanks varied with the reaction time.
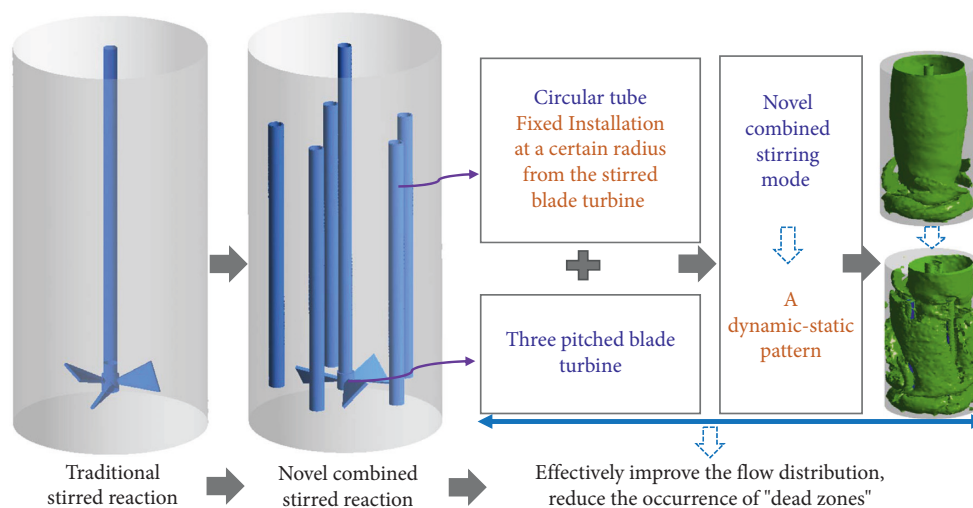

Figure 16: Analysis of dynamic-static coupling strengthening solid-liquid mixing.

4. Conclusion

In the liquid phase oxidation leaching process of chromite submolten salt, a new dynamic-static combined stirring mode was proposed to enhance the chromium leaching process. The flow field simulation analysis of the traditional stirred tank and the dynamic-static combined stirred tank, and the influence of the two stirred tanks on the chromium-leaching rate in the actual reaction were studied. The results showed that the dynamic-static combined stirred tank can improve the flow field distribution, reduce the "swirling" flow pattern and trailing vortex at the tip of the blade, break the symmetric flow field structure, and improve the energy transfer in the stirred tank. From the standpoint of chromite leaching process, the maximum leaching efficiency under the traditional stirred tank was 90%, and the leaching time was as long as 300 min. When the dynamic-static combined stirred tank was adopted, it only took 240 min, and the chromium-leaching rate has reached up to 99 %. This

optimized stirred reactor can provide ideas for intensified research on the chromite-leaching process.

Data Availability

The chart data used to support the findings of this study were supplied by F. C. Qiu under license and so cannot be made freely available. Requests for access to these data should be made to F. C. Qiu, qiufachengandl@126.com.

Conflicts of Interest

The authors declare that they have no conflicts of interest.

Acknowledgments

References

[1] B. Dhal, H. Thatoi, N. Das, and B. Pandey, "Chemical and microbial remediation of hexavalent chromium from contaminated soil and mining/metallurgical solid waste: a review," *Journal of Hazardous Materials*, vol. 250-251, pp. 272–291, 2013.

[2] Z. Sun, Y. Zhang, S. L. Zheng, and Y. Zhang, "A new method of potassium chromate production from chromite and KOH-KNO_3-H_2O binary submolten salt system," *AIChE Journal*, vol. 55, no. 10, pp. 2646–2656, 2009.

[3] M. Bertrand, D. Parmentier, O. Lebaigue, E. Plasari, and F. Ducros, "Mixing study in an unbaffled stirred precipitator using les modelling," *International Journal of Chemical Engineering*, vol. 2012, Article ID 450491, 11 pages, 2012.

[4] E. H. Abdel-Gawad, M. M. Taha, M. A. Abdel-Kawi, G. H. Sedahmed, and M. A. El-Naggar, "Mass and heat transfer in stirred tank equipped with a horizontal tubular cruciform baffle," *Chemical Engineering Research and Design*, vol. 178, pp. 514–522, 2022.

[5] D. J. Lamberto, F. J. Muzzio, P. D. Swanson, and A. L. Tonkovich, "Using time-dependent RPM to enhance mixing in stirred vessels," *Chemical Engineering Science*, vol. 51, no. 5, pp. 733–741, 1996.

[6] T. Nomura, T. Uchida, and K. Takahashi, "Enhancement of mixing by unsteady agitation of an impeller in an agitated vessel," *Journal of Chemical Engineering of Japan*, vol. 30, no. 5, pp. 875–879, 1997.

[7] M. X. Zhang, Y. Y. Hu, W. T. Wang, T. Shao, and Y. Cheng, "Intensification of viscous fluid mixing in eccentric stirred tank systems," *Chemical Engineering and Processing: Process Intensification*, vol. 66, pp. 36–43, 2013.

[8] Z. H. Liu, H. He, J. Zhu, R. Liu, C. Tao, and Y. Wang, "Energy saving and noise reduction of flow mixing performance intensified by rigid-flexible combination impeller: a new impeller applied in mixing with energy," *Asia Pacific Journal of Chemical Engineering*, vol. 10, no. 5, pp. 700–708, 2015.

[9] D. Gu, M. Ye, and Z. Liu, "Computational fluid dynamics simulation of solid-liquid suspension characteristics in a stirred tank with punched circle package impellers," *International Journal of Chemical Reactor Engineering*, vol. 18, no. 9, Article ID 20200026, 2020.

[10] N. F. Nasir, W. R. W. Daud, S. K. Kamarudin, and Z. Yaakob, "Methyl esters selectivity of transesterification reaction with homogenous alkaline catalyst to produce biodiesel in batch, plug flow, and continuous stirred tank reactors," *International Journal of Chemical Engineering*, vol. 2014, Article ID 931264, 13 pages, 2014.

[11] L. Li and B. Xu, "Numerical simulation of hydrodynamics in an uncovered unbaffled stirred tank," *Chemical Papers*, vol. 71, no. 10, pp. 1863–1875, 2017.

[12] L. Li, N. Chen, C. Ning, K. Xiang, and B. Xiang, "CFD simulation of hydrodynamics characteristics in a tank stirred by a hollow self-inducing impeller," *The Canadian Journal of Chemical Engineering*, vol. 96, no. 8, pp. 1837–1848, 2018.

[13] G. R. Kasat, A. R. Khopkar, V. V. Ranade, and A. B. Pandit, "CFD simulation of liquid-phase mixing in solid–liquid stirred reactor," *Chemical Engineering science*, vol. 63, no. 15, pp. 3877–3885, 2008.

[14] N. Sutudehnezhad and R. Zadghaffari, "CFD analysis and design optimization in a curved blade impeller," *International Journal of Chemical Reactor Engineering*, vol. 15, no. 1, Article ID 20160119, 2017.

[15] J. Chen and W. Xiao, "Solids suspension study in a side-entering stirred tank through CFD modeling," *International Journal of Chemical Reactor Engineering*, vol. 11, no. 1, pp. 331–346, 2013.

[16] D. Y. Gu, M. Ye, X. M. Wang, and Z. H. Liu, "Numerical investigation on mixing characteristics of floating and sinking particles in a stirred tank with fractal impellers," *Journal of the Taiwan Institute of Chemical Engineers*, vol. 116, pp. 51–61, 2020.

[17] H. Zhang, H. B. Xu, X. F. Zhang, Y. Zhang, and Y. Zhang, "Pressure oxidative leaching of Indian chromite ore in concentrated NaOH solution," *Hydrometallurgy*, vol. 142, pp. 47–55, 2014.

[18] X. Y. Tang, S. H. He, F. C. Qiu et al., "Intensification of solid–liquid separation by thermal sedimentation in pressure oxidative leaching process of chromite," *Minerals Engineering*, vol. 164, Article ID 106825, 2021.